Final
as sent

CONF-950682--12

PHASE STABILITY IN AUSTENITIC STAINLESS STEELS - NEW APPROACHES, RESULTS, AND THEIR RELATION TO PROPERTIES

J. M. Vitek and S. A. David
Oak Ridge National Laboratory
Oak Ridge, Tennessee 37831-6376
U. S. A.

4th International Conference on Trends in Welding Research
Gatlinburg, Tennessee, June 5-8, 1995

DISCLAIMER

Abstract

In recent years, the phase stability of austenitic stainless steels, and its effect on the mechanical properties of stainless steels, have been the subject of much interest. With the availability of new experimental techniques, new theoretical methods, and new computational procedures, significant advances have been made in understanding, and being able to predict, phase stability and mechanical properties of stainless steel welds. This paper reviews some of these developments, with an emphasis on recent work that has been done at Oak Ridge National Laboratory.

AUSTENITIC STAINLESS STEELS are widely used in a variety of industrial applications in both the cast and wrought condition. In addition, they are used extensively as filler metals in welding operations. Much work has been done over the years in alloy development of stainless steels and in the characterization of stainless steel microstructures and properties. However, in recent years there have been significant new advances made, and insights gained, into the physical metallurgy of these materials. In particular, advanced techniques have led to new information on the phase stability of stainless steels and the influence of the phase stability on mechanical properties. This paper will highlight some of these new advances, with an emphasis on work that has been done in our laboratory on these alloys.

For stainless steel alloys, the phase stability can be influenced by several factors. The schematic diagram in Figure 1 depicts these various factors. They include solidification behavior, the ferrite/austenite solid-state transformation, other high-temperature (approximately 550 to 900°C) phase transformations, and low-temperature (roughly 300 to 550°C) phase transformations. Recent advances in theoretical and experimental methods have led to new developments in understanding and characterizing these factors. Advanced solidification theory has been applied to understand the influence of rapid solidification on phase formation during solidification. New thermodynamic evaluation methods have shown great potential in providing details on the overall phase stability, including details on the influence of composition on phase stability. Finite-difference techniques have been applied to the stainless steel alloy system to gain much insight into the ferrite/austenite transformation behavior. Finally, advanced techniques such as analytical electron microscopy, atom-probe field-ion microscopy, nano-indentation techniques, and specimen miniaturization techniques have provided valuable information on the response of stainless steel microstructures and properties to thermal treatment. All of these new methods and approaches will be described in detail in this presentation.

Solidification Behavior

Weld microstructures are determined, to a large extent, by the solidification behavior. Over the years, the use of constitution diagrams such as the Schaeffler diagram[1] or recent revisions of it[2-4] have been very useful in predicting weld microstructures as a function of alloy composition. These diagrams condense the multicomponent stainless steel alloy compositions into two independent composition variables, namely nickel and chromium equivalents. The usefulness of these types of diagrams lies in the accuracy with which the overall alloy composition can be converted into these simple nickel and chromium equivalents. Much work has been done recently[3,4]

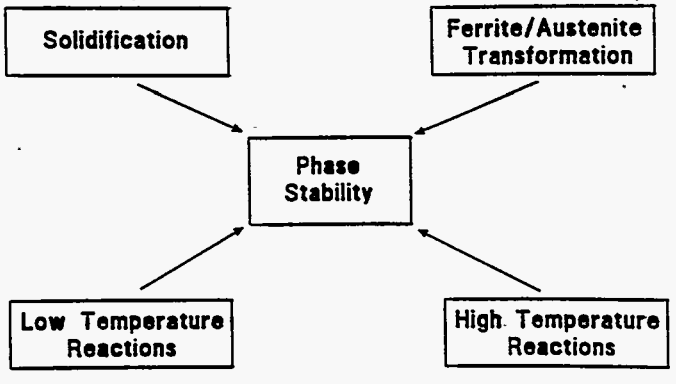

Fig. 1 - Schematic diagram showing the various factors that influence the phase stability in austenitic stainless steels.

toward revising the values of the conversion factors that are used, in order to provide a more reliable diagram that covers a wider range of alloy compositions. These efforts have led to improvements in the overall accuracy of the constitution diagrams.

The use of constitution diagrams has one major drawback, though. Weld microstructure is predicted as a function of weld composition, but processing conditions are not included as a variable. The standard diagrams are traditionally aimed at predicting weld microstructures that are produced under conventional welding conditions. However, the solidification conditions change quite dramatically for laser and other high-energy-density welding techniques, and these often lead to quite different microstructures that are not predicted by the constitution diagrams.[5-15] With the growing use of high-energy-density welding techniques, the impact of these techniques on weld microstructure must be considered more carefully. As an example, Figure 2 shows the weld microstructures that are found after autogenous laser welding of type 316 stainless steels at two different speeds.

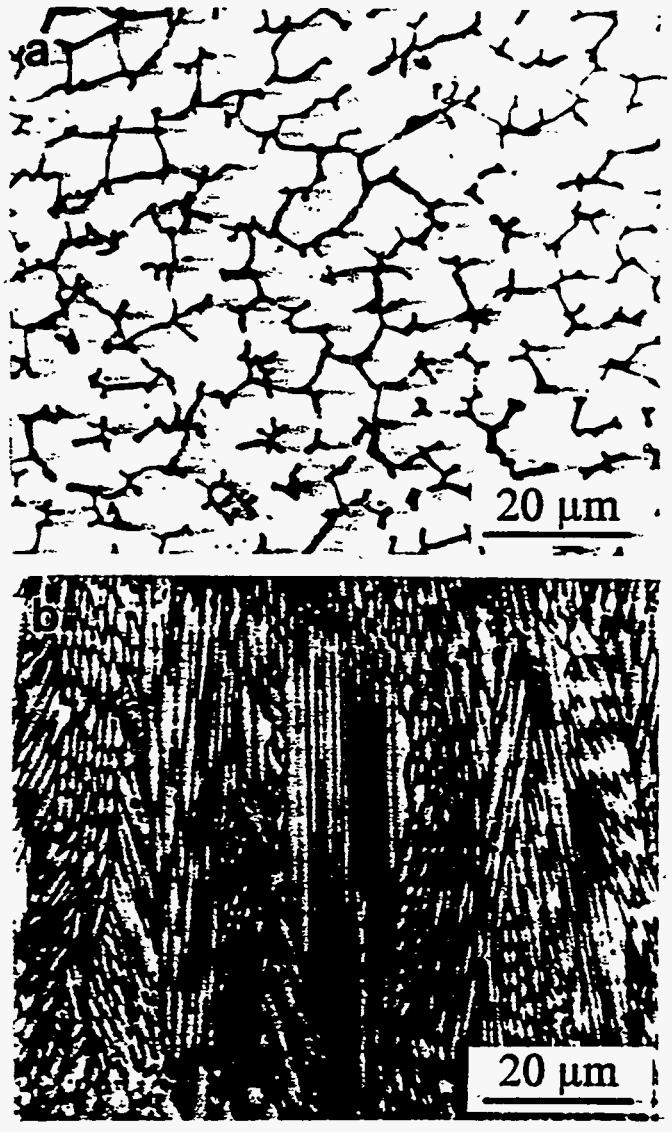

Fig. 2 - Laser welds of type 316 stainless steels at (*a*) low and (*b*) high speeds, showing the change in microstructure that is a result of the change in solidification mode.

At the low laser welding speed [see Figure 2(*a*)], the microstructure is the same as that found after conventional welding. There is approximately 10% residual ferrite in an austenite matrix, and this microstructure is typical of that found in materials that solidify as primary ferrite; most of the ferrite transforms to austenite during cooling. In contrast, after laser welding at a higher speed, the microstructure is fully austenitic [see Figure 2(*b*)] and is a result of a change in the solidification mode to primary austenite solidification. Figure 3 shows the Welding Research Council 1992 constitution diagram[4] with the predicted phase fields. Superimposed on the diagram are five data points corresponding to alloy compositions which are predicted to be two-phase ferrite plus austenite but were found to be fully austenitic after laser welding.[11] These results clearly show that the use of classical constitution diagrams has limited value when applied to welds that have solidified under rapid solidification conditions. Recent work has also shown that changes in solidification mode, which produce these dramatic changes in the weld microstructure, do not necessarily require rapid solidification.[16]

There has been much activity in the theoretical arena to try to explain and understand the solidification behavior under a wide range of solidification conditions.[14,17-20] These studies have examined the relative influence of nucleation behavior and competitive growth between ferrite and austenite solidification. For containerless conditions (e.g., droplet solidification), it has been shown[17,19,20] that homogeneous nucleation is the rate-controlling step and that ferrite nucleation is preferred over austenite nucleation. However, for welding conditions, where heterogeneous rather than homogeneous nucleation takes place, it has been suggested that growth behavior is the controlling factor.[14,18-20] It was found that under many conditions, austenitic growth is faster than ferritic growth. Thus, for heterogeneous nucleation solidification conditions, a change in mode of solidification from primary ferrite to primary austenite is theoretically predicted, in agreement with experimental findings.

A complete understanding of the solidification behavior has not yet been achieved. Furthermore, the influence of the base material on the solidification behavior has not yet been addressed.

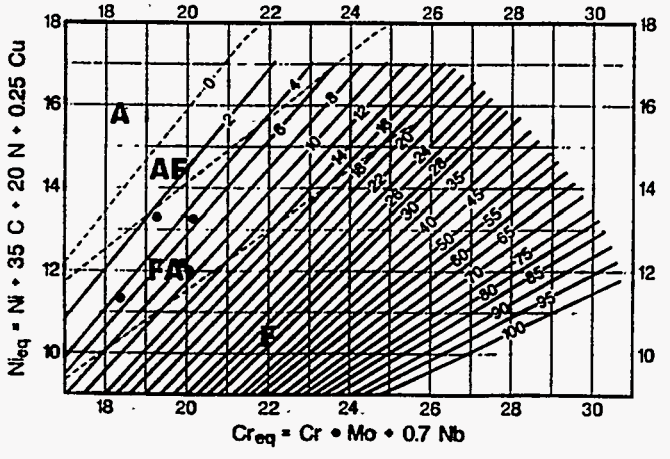

Fig. 3 - Welding Research Council 1992 constitution diagram from ref. 4 with superimposed compositions that showed fully austenitic microstructures after laser welding.

ITEK – DAVID

2

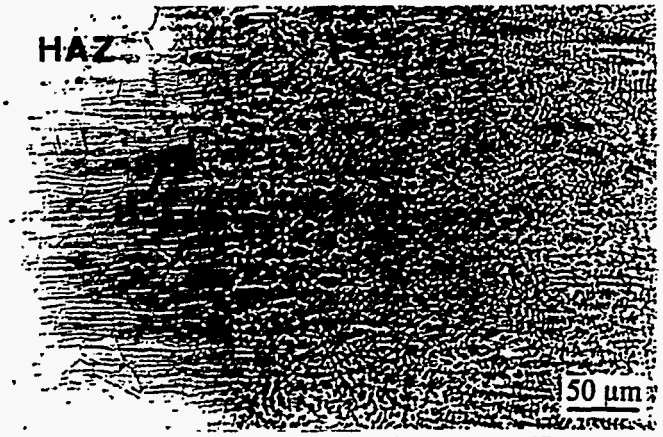

Fig. 4 - The heat-affected zone (HAZ)/fusion zone (FZ) interface of a type 304 stainless steel laser weld showing the presence of ferrite in the formerly fully austenitic HAZ.

Figure 4 shows the heat-affected zone (HAZ)/fusion zone (FZ) interface of a type 304 stainless steel autogenous laser weld. The base material was solutionized prior to welding to produce a fully austenitic microstructure. In the area immediately adjacent to the FZ, some intergranular ferrite formation can be found, as indicated by the arrow. The presence of ferrite clearly indicates that the fully austenitic microstructure partially transformed to ferrite during heating. The kinetics of this reaction are not documented, and the influence of the presence (or absence) of ferrite in the base material on the solidification behavior is also not understood. Further work in this area is clearly needed to determine if ferrite in the HAZ has an influence on the solidification behavior in the FZ. As described later in this paper, modeling of the ferrite/austenite transformation may be very helpful in providing valuable information on the nature and kinetics of ferrite formation in the HAZ.

Thermodynamic Calculations of Phase Stability in Austenitic Stainless Steels

In the last 15 years, tremendous advances have been made in the ability to calculate the thermodynamic properties of phases. This, in turn, has led to significant improvement in the ability to calculate phase stability as a function of alloy composition and thermal conditions. These calculation procedures rely on actual thermodynamic data and not empirical relationships. Simplified models are used to evaluate the free energy of competing phases and to predict, as a result, the stable phases under any given conditions. Software codes are available that can be used to calculate the appropriate thermodynamic properties. One such program is the ThermoCalc™ program that has been developed by a group at the Royal Institute of Technology in Stockholm, Sweden.[21] The availability of these types of programs allows one to evaluate phase stability in much greater detail, and with much greater accuracy, than has been possible in the past.

The thermodynamic software codes can readily handle multicomponent systems. A sample calculation of a vertical section of the equilibrium phase diagram of a six-component system (Fe-Cr-Ni-Mn-Si-C) is shown in Figure 5. In this diagram,

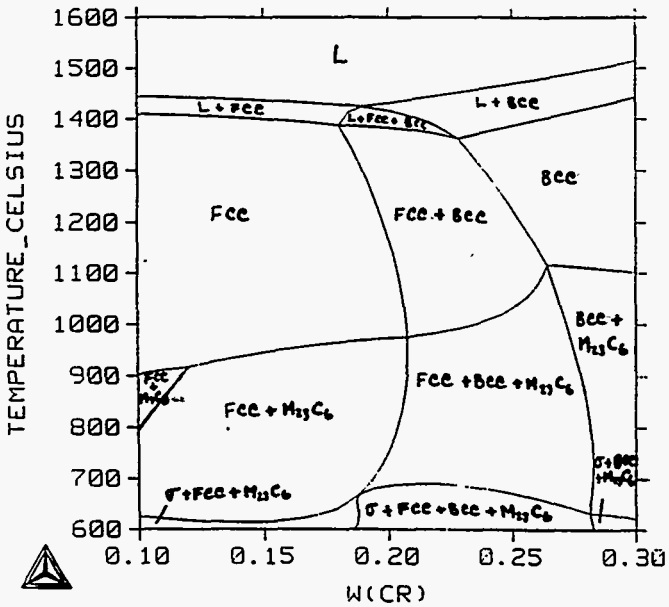

Fig. 5 - Calculated vertical section of an Fe-Cr-Ni-Mn-Si-C alloy with Cr and Ni varying and Fe, Mn, Si, and C fixed at 0.67, 0.016, 0.0044, and 0.0006 wt fraction, respectively. The Cr content is given in wt fraction, ranging from 0.1 to 0.3.

the chromium and nickel are varied while the iron, manganese, silicon, and carbon are fixed at 0.67, 0.016, 0.0044, and 0.0006 wt fraction, respectively. The vertical section shows the extent of the various phase fields, and more detailed information on the relative amounts of the phases and their compositions can be easily obtained as well. In this particular diagram, information such as the range for primary ferrite solidification (under equilibrium conditions), or the temperature range for stability of sigma phase, $M_{23}C_6$, or any other phase, can be readily extracted. Such diagrams can be constructed as a function of any component, and this information can be very useful in ascertaining the influence of various components on the overall phase stability. As discussed in the next section, the information from these types of calculations can also be used in other analyses, such as the evaluation of the diffusion-controlled ferrite/austenite phase transformation.

Modeling the Ferrite-to-Austenite Transformation in Austenitic Stainless Steels

As shown in the vertical phase diagram section in Figure 5, the stability of the ferrite [body-centered cubic (BCC)] decreases with decreasing temperature while the austenite [face-centered cubic (FCC)] phase stability increases. For a chromium content of approximately 23% (wt %) or greater, a fully ferritic microstructure exists at elevated temperatures, but as the temperature is lowered, the ferrite transforms to austenite. In most cases, this transformation is diffusion controlled. Recently, efforts have been made to model this transformation.[22-29] Such modeling efforts can provide much information that is difficult or impossible to obtain experimentally. For example, the transformation behavior in the HAZ immediately adjacent to the FZ can be determined. Direct microstructural observation such as that shown

in Figure 4 indicates that the reverse austenite-to-ferrite transformation must take place during elevated-temperature exposure of the HAZ, but the room-temperature microstructure does not provide any details on the rate and extent of the transformation. Instead, the interpretation of the microstructure is complicated by the fact that the ferrite that forms during exposure to the highest temperatures partially transforms back to austenite during cooling. Thus, experimental evaluation of the transformation is clouded by the imperfect quenching from elevated temperatures. In addition, modeling is not composition specific so, unlike experimental studies which are strictly valid for the composition that is tested, modeling can be extended to any composition. Modeling can also provide details such as the compositions of the phases and the presence of gradients in the phase compositions.

Initial modeling efforts[22-24] were aimed at studying the isothermal transformation behavior of a casting stainless steel at 1100°C. These efforts were expanded to other alloys, more typical of weld filler metals, and to a wider range of aging temperatures, from 700 to 1300°C.[25-29] A finite-difference method was used to follow the diffusion-controlled transformation in the ternary Fe-Cr-Ni system using standard computational techniques. A typical result is shown in Figure 6 for the aging behavior at 1100°C for two alloys, Fe-21.9Cr-10.35Ni and Fe-21Cr-11.3Ni (in wt %). The initial ferrite content was 10%, and the initial ferrite and austenite compositions were set at values typical of as-welded microstructures. The results clearly show the progress of the transformation. Interestingly, the transformation often does not proceed in a direct manner toward final equilibrium. For example, in Figure 6, for the Fe-21Cr-11.3Ni alloy, the ferrite content increases from 10 to over 12% before finally decreasing to the equilibrium level of less than 4%. The corresponding changes in ferrite and austenite chromium compositions are shown in Figure 7. Once again, the approach to final equilibrium is not direct, and the changes in composition are found to reverse themselves under certain conditions. The reader is referred to other publications for additional details on these modeling studies.[25-28]

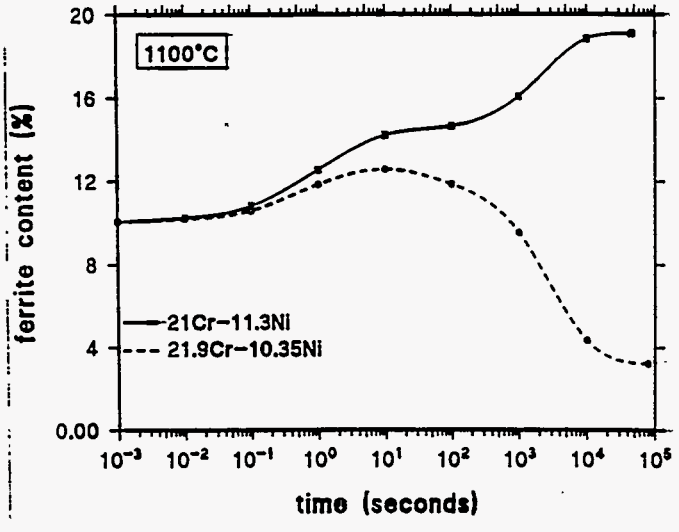

Fig. 6 - Calculated ferrite content as a function of aging time at 1100°C for two Fe-Cr-Ni ternary alloys.

Such modeling calculations need not be restricted to isothermal aging conditions. In fact, it is desirable to extend these calculations to nonisothermal conditions in order to follow the phase transformation behavior in a weldment during cooling after solidification. Eventually, it would be desirable to model the transformation behavior in the HAZ as well, where the material is subjected to one or more thermal cycles. Such thermal histories can be readily incorporated into the modeling code. An example is given in Figure 8, where the (residual) ferrite content is plotted as a function of temperature for a range of constant cooling rates from 0.1 to 100°C/s over the temperature interval from 1300 to 700°C. The starting condition was equilibrium at 1300°C, and the overall alloy composition was Fe-21Cr-11.3Ni. Also shown is the equilibrium ferrite content as a function of temperature. The equilibrium ferrite content decreases with decreasing temperature from 1300 to approximately 1025°C. Over the temperature range from 1025 to roughly 900°C, austenite is the only stable phase, and at lower temperatures, ferrite exists once again as a stable phase. The calculations show that deviations from equilibrium occur at all cooling rates over the entire temperature range. If one ignores the increase of ferrite stability below 900°C, then the

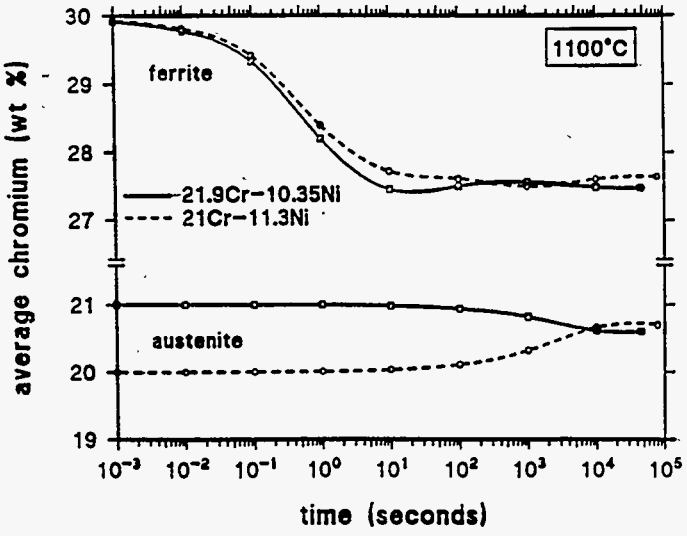

Fig. 7 - Calculated average ferrite and austenite chromium concentrations as a function of aging time at 1100°C for two Fe-Cr-Ni ternary alloys.

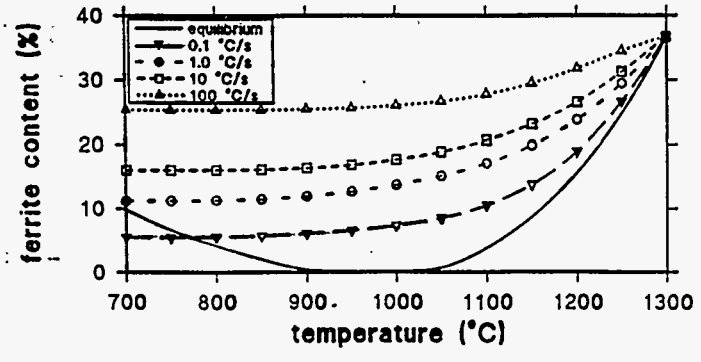

Fig. 8 - Calculated ferrite content as a function of temperature during cooling from 1300°C at various constant cooling rates. The equilibrium ferrite content versus temperature is also given.

deviations from equilibrium increase with decreasing temperature and increasing cooling rate, as is expected. To ignore the resurgence of equilibrium ferrite at lower temperatures is reasonable since, as shown elsewhere,[29] the increased ferrite stability at low temperatures has little influence on the microstructural development during the latter stages of cooling. This is because the composition profiles that have been established and that lead to ferrite dissolution at higher temperatures during cooling are difficult to reverse. The calculations show how much residual ferrite can be expected after cooling, as a function of the cooling rate. The different cooling rates can be correlated with different welding conditions. Similarly, the ferrite and austenite compositions can be determined as a function of temperature and cooling rate.[25-29]

The recent modeling efforts have considered ternary systems of iron-chromium-nickel to simulate austenitic stainless steel compositions. The evaluation of ternary systems allows for added flexibility in the phase equilibria at the interface that is characteristic of multicomponent systems and is absent when considering only binary systems.[25,27] As a result, several unusual effects were found for the ternary system models.[22-29] These included the initial growth of ferrite followed by subsequent dissolution at longer exposure times, or the reverse, namely initial dissolution followed by growth. Reversals in the composition changes of the ferrite and austenite were also found. Finally, for calculations for constant cooling conditions, it was found that higher cooling rates do not always result in greater deviations from equilibrium.[26] Thus, the models of ternary systems showed that the kinetics and transformation behavior may be considerably more complicated if realistic multicomponent systems are modeled rather than simplified binary systems.

High-Temperature (> 550° C) Phase Stability in Austenitic Stainless Steels

In addition to the ferrite/austenite transformation that has been discussed in detail above, austenitic stainless steels undergo two other elevated-temperature transformations, the formation of $M_{23}C_6$ carbides and sigma phase formation. Both of these transformations have significant effects on the mechanical properties of austenitic stainless steel welds. Sigma phase is a brittle phase that is known to have a deleterious impact on mechanical properties. The austenite-to-sigma transformation is quite sluggish, but the sigma formation takes place at an accelerated rate when ferrite is present. This is clearly demonstrated by the TTT diagrams shown in Figure 9 for type 308 stainless steel in the homogenized [see Figure 9(*a*)] and the as-welded [see Figure 9(*b*)] conditions. In the first case, the initial microstructure is fully austenitic, and sigma phase formation requires over 5000 h of aging at 750° C. In contrast, sigma phase is found within 20 h at 750° C in the as-welded condition, where residual ferrite is present. The sigma phase formation in welded austenitic stainless steels was examined in detail, and it was concluded that sigma phase formation is nucleation controlled and the presence of ferrite accelerates the nucleation rate dramatically.[30]

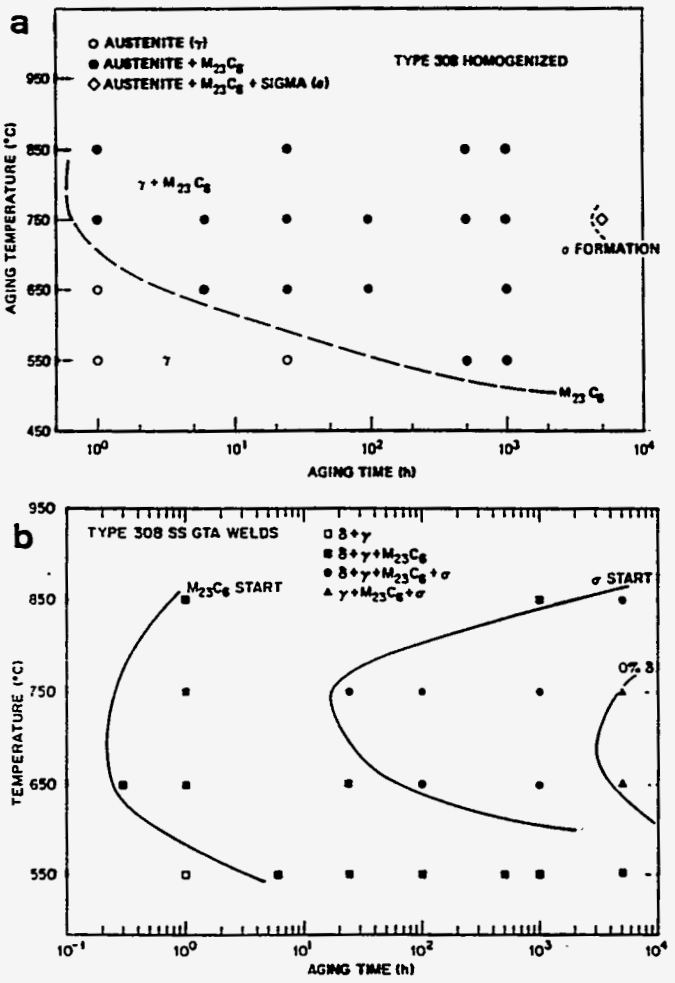

Fig. 9 - Comparison of experimentally determined TTT diagrams for (*a*) homogenized and (*b*) as-welded type 308 stainless steel.

Carbide formation, in the form of the chromium-rich, fcc, $M_{23}C_6$ carbide, takes place within hours over the temperature range of 650 to 850° C (see Figure 9). This carbide forms preferentially at the ferrite/austenite interface. With extended aging, some ferrite may transform to austenite, or to sigma phase, but the carbide that forms early with elevated-temperature exposure outlines the original ferrite/austenite interface. In austenitic stainless steel weldments where the ferrite is the primary solidification phase, the ferrite exists as a continuous network, and, therefore, the carbide that outlines the ferrite also forms such a continuous network. In studies on interrupted creep specimens,[31] it was found that the carbide network has a more deleterious effect than sigma phase formation in that it leads to extensive crack formation and reduced creep ductility and creep life. Figure 10 shows a scanning electron micrograph of an interrupted creep specimen in which cracks are found along the carbide network. The carbide network and the cracks are often significantly removed from the sigma phase. It has been shown that minor additions of titanium, boron, and phosphorous can lead to significant improvements in the creep properties of austenitic stainless steels.[32-36] More recent work has identified the mechanism by which titanium improves the creep properties.[31,37,38]

VITEC - DAVID

Fig. 10 - Crack formation along carbide network in interrupted creep sample of type 308 stainless steel.

With titanium additions, titanium carbides form easily at elevated temperatures and are uniformly distributed within the microstructure. Therefore, the titanium eliminates the formation of the $M_{23}C_6$ carbide network, and this leads to a significant improvement in creep life and creep ductility. Recent work has also attempted to identify the role of boron in improving the creep properties.[39-40] This work has shown that the boron preferentially segregates to the $M_{23}C_6$ carbide, but the exact mechanism by which this leads to an improvement in properties is yet to be determined.

Low-Temperature (< 550° C) Phase Stability in Austenitic Stainless Steels

Below approximately 550°C, two new phase transformations become important. These are ferrite decomposition into α and α′, and G-phase formation. In addition, $M_{23}C_6$ carbide formation, as found at higher temperatures, also occurs. However, sigma formation does not take place in the low-temperature regime. The exact temperatures of these reactions, and the extent to which they occur, are composition sensitive. These transformations have potentially significant impacts on the mechanical properties. In fact, the embrittlement that develops after aging in this temperature range has the generic description "475°C embrittlement." Much work has been done in recent years to help identify the microstructural development that leads to embrittlement and the overall degradation of mechanical properties. A summary of recent work can be found in the proceedings of a conference on this topic.[41] However, the specific contribution of each transformation still needs to be determined.

At temperatures below approximately 500°C, the ferrite phase decomposes into an iron-rich α phase and a chromium-rich α′ phase.[41,42] This reaction most often takes place by a spinodal decomposition mechanism. The decomposition into α and α′ is quite rapid, requiring only a few hours at temperatures of 400°C or more. A typical transmission electron micrograph of ferrite that has decomposed spinodally after aging at 475°C is shown in Figure 11(*a*). With longer aging times, fine precipitation of G-phase, a nickel-rich silicide, is observed,[42-45] as shown in Figure 11(*b*). The G-phase precipitates preferentially on dislocations within the ferrite, but fine and homogeneous

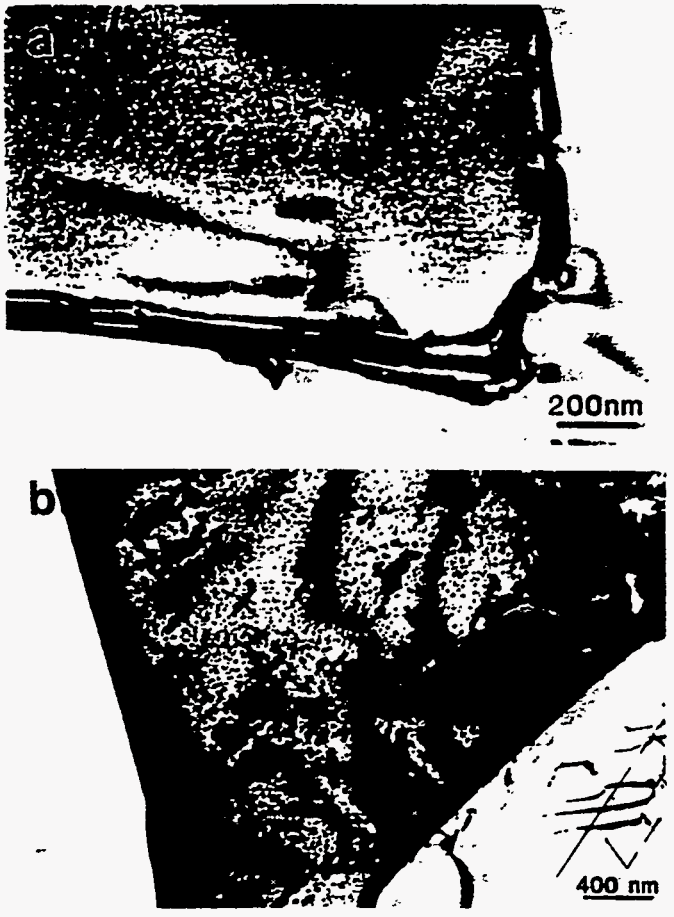

Fig. 11 - Transmission electron micrographs showing (*a*) α and α′ formation in ferrite phase of type 308 stainless steel weld aged for 100 h at 475°C and (*b*) fine precipitation of G-phase in ferrite of type 308 stainless steel weld aged for 500 h at 475°C.

precipitation of G-phase is also found.[42,45] Finally, as found at higher temperatures, chromium-rich $M_{23}C_6$ carbide forms at the ferrite/austenite interface.

The consequences of these three phase transformations are quite dramatic in terms of mechanical properties, and in particular, toughness properties. Impact properties of aged weldments were studied in detail,[42] and representative curves of Charpy impact energy versus test temperature for welds aged at 475°C are shown in Figure 12. Embrittlement occurs in two forms: an upward shift of approximately 100°C in the ductile-brittle transition temperature after short aging times and a significant decrease of more than 50% in the upper-shelf energy after longer aging times. A corresponding increase in the hardness of the residual ferrite islands was also found.[42,46] Unfortunately, the kinetics of the various phase transformations that occur are such that the transformations overlap so that a clear identification of the role of each transformation has not been possible to date. Nonetheless, evidence suggests that each transformation is undesirable in that each makes a contribution to the overall embrittlement.[42,47]

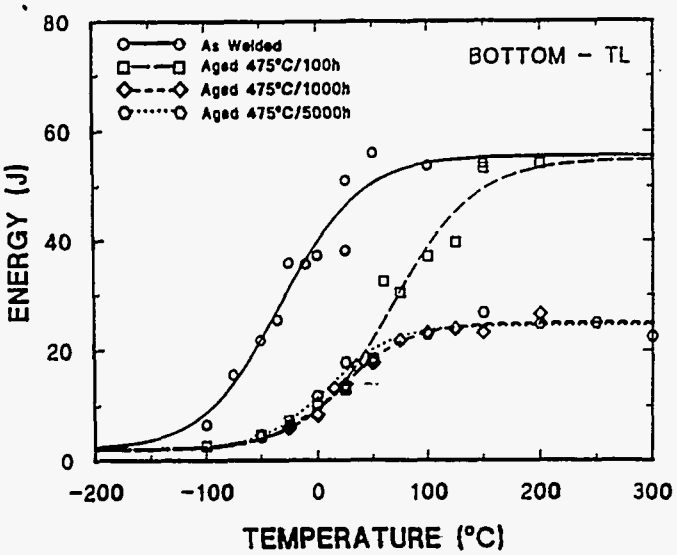

Fig. 12 - Charpy impact energy of type 308 stainless steel weld aged at 475° C.

Summary

Several new approaches have been explored in recent years to follow the phase stability in austenitic stainless steels. These approaches include thermodynamic analysis of phase stability, advanced solidification theory, numerical modeling procedures for studying diffusion-controlled transformation behavior, and experimental investigations of phase transformation behavior and mechanical properties. Recent findings in each of these areas have been reviewed. New developments in these methods and techniques, alone and in combination with one another, show promise as a means for accurately predicting and understanding the microstructure, properties, and thermal response of austenitic stainless steel welds.

Acknowledgments

This research was sponsored by the Division of Materials Sciences, U.S. Department of Energy, under contract DE-AC05-84OR21400 with Lockheed Martin Energy Systems. The authors would also like to thank Drs. E. A. Kenik and G. M. Goodwin for their helpful comments and K. Spence for technical editing.

References

1. A. L. Schaeffler, *Met. Prog.* 56, 680-680B (1949).
2. W. T. DeLong, *Weld. J.* 53(7), 273s-286s (1974).
3. T. A. Siewert, C. N. McCowan, and D. L. Olson, *Weld. J.* 67(12), 289s-298s (1988).
4. D. J. Kotecki and T. A. Siewert, *Weld. J.* 71(5), 171s-178s (1992).
5. S. A. David and J. M. Vitek, in *Lasers in Metallurgy*, eds. K. Mukherjee and J. Mazumder (The Metallurgical Society, Warrendale, Pennsylvania, U. S. A.), 247-254 (1982).
6. S. Kou and Y. Le, *Metall. Trans. A* **13A**, 1141-1152 (1982).
7. J. M. Vitek, A. Das Gupta, and S. A. David, *Metall. Trans. A* **14A**, 1833-1841 (1983).
8. S. Katayama and A. Matsunawa, in *Proc. of Mater. Processing Symp.*, Vol. 44 (Laser Inst. of America, ICALEO), 60-67 (1984).
9. S. Katayama and A. Matsunawa, in *Proc. Int'l. Conf. on Applic. of Lasers and Electro-Optics*, (Laser Inst. of America, ICALEO), 19-25 (1985).
10. J. C. Lippold, *Weld. J.* **64(5)**, 127s-136s (1985).
11. S. A. David, J. M. Vitek, and T. L. Hebble, *Weld. J.* 66(10), 289s-300s (1987).
12. S. Venkataraman and J. H. Devletian, *Weld. J.* **67(6)**, 111s-118s (1988).
13. Y. Nakao, K. Nishimoto, and W. P. Zhang, in *Proc. 4th Int'l. Colloq. on Welding and Melting by Electron and Laser Beams*, eds. M. Contré and M. Kuncevic (French Inst. Weld.), 673-680 (1988).
14. J. W. Elmer, S. M. Allen, and T. W. Eagar, *Metall Trans. A* **20A**, 2117-2131 (1989).
15. J. A. Brooks, M. I. Baskes, and F. A. Greulich, *Metall. Trans. A* **22A**, 915-926 (1991).
16. H. K. D. H. Bhadeshia, S. A. David, and J. M. Vitek, *Mater. Sci. Technol.* 7, 686-698 (1991).
17. T. F. Kelly, M. Cohen, and J. B. VanderSande, *Metall. Trans. A* **15A**, 819-833 (1984).
18. M. Bobadilla, J. Lacaze, and G. Lesoult, *J. Cryst. Growth* 89, 531-544 (1988).
19. W. Löser and D. M. Herlach, *Metall. Trans. A* **23A**, 1585-1591 (1992).
20. T. Koseki, PhD. Thesis, Massachusetts Institute of Technology, Cambridge, Massachusetts, U. S. A. (1994).
21. B. Sundman, B. Jansson, and J-O. Andersson, *CALPHAD* 9, 153-190 (1985).
22. M. Kajihara, C. B. Im, and M. Kikuchi, in *Stainless Steels '91, International Conference on Stainless Steels*, Vol. 1, (Iron and Steel Inst. Japan, Tokyo) 677-684 (1991).
23. Masanori Kajihara, Chang-Bim Lim, and Makoto Kikuchi, *Iron Steel Inst. Jpn. Int'l.* **33**, 498-507 (1993).
24. M. Kajihara and M. Kikuchi, *Acta Metall. Mater.* **41**, 2045-2059 (1993).
25. J. M. Vitek, S. A. Vitek, and S. A. David, in *Solid→Solid Phase Transformations*, eds. W. C. Johnson, J. M. Howe, D. E. Laughlin and W. A. Soffa (The Minerals, Metals and Materials Society, Warrendale, Pennsylvania, U. S. A.), 201-206 (1994).
26. J. M. Vitek and S. A. Vitek, in *Phase Transformations During the Thermal/Mechanical Processing of Steel*, eds. E. B. Hawbolt and S. Yue (Metallurgical Society of Canadian Inst. Mining Metallurgy and Petroleum, Montréal, Canada), 431-443 (1995).
27. J. M. Vitek, S. A. Vitek, and S. A. David, *Metall. Trans. A* **26A**, 2007-2025 (1995).
28. J. M. Vitek, S. A. Vitek, and S. A. David, in *Proc. 4th Int'l. Conf. on Trends in Welding Research, Gatlinburg, Tennessee, U. S. A., June 5-8, 1995.*

29. J. M. Vitek and Y. S. Iskander, in *Proc. 3rd Int'l. Seminar on Numerical Analysis of Weldability, Graz, Austria, Sept. 25-27, 1995.*
30. J. M. Vitek and S. A. David, *Weld. J.* 65, 106s-111s (1986).
31. J. M. Vitek, S. A. David, and V. K. Sikka, *Weld. J.* 71, 421s-434s (1992).
32. N. C. Binkley, R. G. Berggren, and G. M. Goodwin, *Weld. J.* **53(2)**, 91s-95s (1974).
33. R. T. King, J. O. Stiegler, and G. M. Goodwin, *Weld. J.* **53(7)**, 307s-313s (1974).
34. J. O. Stiegler, R. T. King, and G. M. Goodwin, *J. Eng. Mater. Technol.* **97(3)**, 245-250 (1975).
35. R. L. Klueh and D. P. Edmonds, *Weld. J.* **65(1)**, 1s-7s (1986).
36. R. L. Klueh and D. P. Edmonds, *Weld. J.* **65(6)**, 156s-162s (1986).
37. J. M. Vitek and S. A. David, *Weld. J.* **63(8)**, 246s-253s (1984).
38. J. M. Vitek and S. A. David, *Metall. Trans. A* **18A**, 1195-1201 (1987).
39. S. S. Babu, S. A. David, J. M. Vitek, and M. K. Miller, *Appl. Surf. Sci.* **87**, 207-215 (1995).
40. S. S. Babu, S. A. David, J. M. Vitek, and M. K. Miller, accepted for publication in *Metall. Trans. A* (1995).
41. Int'l. Workshop on Intermediate Embrittlement Processes in Duplex Stainless Steels, *Mater. Sci. Technol.* **6** (1990).
42. J. M. Vitek, S. A. David, D. J. Alexander, J. R. Keiser, and R. K. Nanstad, *Acta Metall.* **39**, 503-516 (1991).
43. M. Vrinat, R. Cozar, and Y. Meyzaud, *Scr. Metall.* **20**, 1101-1106 (1986).
44. J. M. Vitek, *Metall. Trans. A* **18A**, 154-156 (1987).
45. M. K. Miller and J. Bentley, in *Environmental Degradation of Materials in Nuclear Power Systems - Water Reactors*, eds. G. J. Theus and J. R. Weeks (TMS-AIME, Warrendale, Pennsylvania, U. S. A.), 341-349 (1988).
46. S. A. David, J. M. Vitek, J. R. Keiser, and W. C. Oliver, *Weld. J.* **66**, 235s-240s (1987).
47. J. M. Vitek, S. A. David, and D. J. Alexander, in *Microstructural Science Vol. 21: Metallographic Investigations of Corrosion, Deformation and Fracture of Engineering Materials*, eds. C. R. Brooks and M. R. Louthan, Jr. (ASM-International, Materials Park, Ohio, U. S. A.), 3-12 (1994).